Lateral evolution of the rift-to-drift transition in the South China Sea: Evidence from multi-channel seismic data and IODP Expeditions 367&368 drilling results

Weiwei Ding, Zhen Sun, Geoffroy Mohn, Michael Nirrengarten, Julie Tugend, Gianreto Manatschal, Jiabiao Li

Lateral evolution of the rift-to-drift transition in the South China Sea: Evidence from multi-channel seismic data and IODP Expeditions 367&368 drilling results

Weiwei Ding [a,b,*], Zhen Sun [c,**], Geoffroy Mohn [d], Michael Nirrengarten [d], Julie Tugend [e,f], Gianreto Manatschal [g], Jiabiao Li [a]

[a] *Key Laboratory of Submarine Geosciences, State Oceanic Administration, Second Institute of Oceanography, Ministry of Natural Resources, Hangzhou 310012, China*
[b] *Shanghai Jiao Tong University, School of Oceanography, Shanghai 20030, China*
[c] *CAS Key Laboratory of Ocean and Marginal Sea Geology, South China Sea Institute of Oceanology, Chinese Academy of Sciences (CAS), Guangzhou 510301, China*
[d] *Laboratoire Géosciences et Environnement Cergy (GEC), Maison Internationale de la Recherche, Université de Cergy-Pontoise, Paris 95000, France*
[e] *Sorbonne Université, CNRS-INSU, Institut des Sciences de la Terre Paris, ISTeP UMR 7193, F-75005 Paris, France*
[f] *Total SA, R&D department CSTJF, 64000 Pau, France*
[g] *Institut de Physique du Globe de Strasbourg, Université de Strasbourg, Strasbourg-CNRS, F-67084, France*

A B S T R A C T

The South China Sea margins represent a critical natural laboratory to study the processes and parameters controlling the rift-to-drift transition. High quality seismic data previously suggested the occurrence of a relatively sharp transition between the continental and oceanic domains, a hypothesis recently validated by the results of the IODP Expedition 367&368 drilled in the northern South China Sea distal margin. Drilling results in this transition cored Mid-Ocean Ridge type basaltic basement (Site U1502), while its lateral equivalent showed continental affinities (Site U1499). Seismic data document the lateral evolution of this narrow transition zone (∼15 to 25 km wide) and tectono-magmatic context related to breakup. A short-period magmatic event occurred during the latest stage of continental rifting and intruded the edge of the thinned continental crust, triggering crustal breakup and onset of steady-state seafloor spreading. The architecture of the transitional domain documented in this work is in marked contrast with those interpreted as either magma-starved or magma-rich at breakup time, suggesting that the continental margin of the SCS is intermediate between the classical end-member magmatic archetypes. We propose that the magmatic event triggering continental breakup is related to decompression melting linked to the ascending asthenosphere. It is assumed that this event was rapid at geological time scale (<10 Ma) and was favored by a high mantle temperature.

© 2019 The Author(s). Published by Elsevier B.V. This is an open access article under the CC BY-NC-ND license (http://creativecommons.org/licenses/by-nc-nd/4.0/).

1. Introduction

New observations and the acquisition of new data are crucial to describe the architecture and nature of transitional domains lying between continental and oceanic crusts and understand the evolution of the thermal state and strength of the lithosphere during breakup and subsequent onset of seafloor spreading. Transitional domains have been investigated in both magma-rich and magma-poor rifted margins thanks to data sets from the Oceanic Drilling Program (ODP) (e.g. Larsen and Saunders, 1998), high-resolution multichannel seismic (MCS) data (e.g. Péron-Pinvidic et al., 2007) and field studies in fossil analogues (e.g. Abdelmalak et al., 2015). These observations enabled the development of conceptual ideas inspired by analogue and numerical modeling (e.g. Lavier and Manatschal, 2006; Brune et al., 2014). Magma-rich COTs, as interpreted in the South Atlantic and Northwest Australian margins (e.g. Franke et al., 2010; Stica et al., 2014), are characterized by Seaward Dipping Reflector sequences (SDRs). SDRs are built by the stacking of landward flowing basaltic melts interbedded with sediments during breakup. Their formation is either related to landward dipping faults and/or related to oceanward flexure (Paton et al., 2017). SDRs are typically floored by high-velocity bodies (Vp ∼ 7.2-7.6 km/s) that are interpreted to result from magmatic underplat-

ing/intrusions (e.g. White et al., 1992). Magma-poor transitional domains show evidence for hyper-extended continental crust, and locally also of exhumed sub-continental serpentinized mantle, as exemplified by the Iberia-Newfoundland margins (e.g., Boillot et al., 1980; Whitmarsh et al., 2001). However, this bipolar vision of rifted margin is an over simplification and case studies are expected to exist in-between.

In the northern South China Sea (SCS) margin neither SDRs nor exhumed mantle have been drilled, dredged or observed in seismic sections. However, evidence for a high-velocity layer (HVL) in the lower crust (Yan et al., 2001; Chiu, 2010), magmatic additions in the continental slope (Zhao et al., 2016; Fan et al., 2017) and occurrence of detachment faults affecting the hyper-extended crust have been described (Franke et al., 2014; Gao et al., 2015; Zhao et al., 2018). The South China Sea margin does not resemble the classical end-member magmatic archetypes and has recently been recognized as an "intermediate" type (Larsen et al., 2018) based on the results of the International Ocean Discovery Program (IODP) Expeditions 367&368. Seven sites, spanning from a basement high in the distal margin to the initial oceanic crust, have been successfully cored (Sun et al., 2018). In complement to Larsen et al. (2018), here we interpret four crustal-scale MCS profiles to investigate the deformation pattern, magmatic architecture and lateral variability of the COT architecture of the northern SCS. We tentatively characterize the location, amount, and timing of magmatic additions that occurred during breakup, and aim to document further the mechanisms controlling the rift-to-drift transition in the northern SCS by focusing on its tectono-magmatic evolution.

2. Geological setting

Since the Triassic, the realm from which the SCS developed was in a convergent setting caused by the subduction of the paleo-Pacific (Taylor and Hayes, 1983). During the Paleogene, the paleo-stress field changed from compression to extension as a result of subduction rollback (Taylor and Hayes, 1983). This resulted in episodic rifting events with uplifting shoulders and local erosion that continued into Cenozoic time. The extensional tectonics of the Cenozoic is evidenced by the development of basins bounded by serial, parallel, to en echelon faults, some of these structures being interpreted as long offset detachment faults (Franke et al., 2014; Zhao et al., 2018). Two main rift events can be distinguished: an earlier Paleocene to Eocene and a late Eocene to early Miocene (Cullen et al., 2010). The former event was widespread and can be identified in nearly all sedimentary basins in the continental shelf. Conversely, the latter event resulted in seafloor spreading and the formation of the SCS.

A model for the opening scenario of the SCS was first proposed by Taylor and Hayes (1983) and Briais et al. (1993) on the basis of the magnetic anomalies, indicating that seafloor spreading occurred between 32 and 16 Ma. In contrast, Barckhausen et al. (2014) suggested a cessation age of 20.5 Ma based on more recent ship-borne magnetic data. Although there is 3–4 Myr differences in the cessation time, most authors agree that seafloor spreading occurred in the East Sub-basin first, followed by a southward ridge jump and a re-orientation of the spreading geometry from a westward to a southwestward ridge propagation (Briais et al., 1993; Ding et al., 2018).

Shipboard results of microfossil biostratigraphy and palaeomagnetic results from the IODP Expedition 349 (Li et al., 2015) and the IODP Expeditions 367&368 (Sun et al., 2018), combined with analysis on recently-acquired deep tow magnetic anomalies (Li et al., 2014), and $^{40}Ar/^{39}Ar$ dating of basalts near the fossil spreading ridge (Koppers, 2014), have shown that seafloor spreading occurred between ~30 Ma and 16 Ma, supporting age models proposed by

Taylor and Hayes (1983) and Briais et al. (1993). The cessation time coincides with the onset of collision between Palawan and Borneo and Mindoro-Central Philippines (Cullen et al., 2010), suggesting a causal relationship between the two events.

The seismic sections presented here mainly run across the distal domain of the northern SCS margin documenting the structure of the Continent-Ocean Transition (COT). To the NW, the sections image the most distal/southern part of the Pearl River Mouth Basin (PRMB) and adjacent oceanic crust. The PRMB consists of Cenozoic basins that formed during a syn-rift stage (~53 Ma to 32 Ma), followed by a post-rift stage (32 Ma to 10.5 Ma), and a final rejuvenation stage (10.5 Ma to recent) (Clift and Lin, 2001; Wang et al., 2018). The crustal architecture of the southern part of the PRMB has been well documented using wide-angle seismic surveys and presents a seaward crustal thinning from 24 km to 12 km (e.g. Yan et al., 2001). The Cenozoic rift extension is accommodated by detachment faults forming deep basins with ramp syncline and roll-over anticline structures (Zhao et al., 2018; Wang et al., 2018).

3. Reflection seismic, drill hole data and interpretational approach

3.1. Reflection seismic data and processing

Four MCS sections have been interpreted in this study (for locations of sections see Fig. 1). Seismic sections N2, N3 and N4 were obtained during the national oceanic project cruise by the Second Institute of Oceanography, Ministry of Natural Resources, in 2004. The sections were obtained by *R/V Tanbao* through 480 channels, 6237.5 m-long streamer, and were recorded in Seg-D format at 2 ms sampling intervals and 12 second (s) trace length. The shot interval is 37.5 m. Seismic section SO49-17 was obtained during the "Joint Sino-German South China Sea Cruise" in 1987. The section was obtained by *R/V SONNE* through 48 channels. Pre-stack processing of the seismic data includes amplitude compensation, static correction, gain and mute analysis, predictive deconvolution, multiple attenuation, velocity analysis, residual static corrections and frequency filtering. Post-stack deconvolution, band-pass and coherency filtering are applied to the stacked data, followed by a finite-difference migration.

3.2. Drill hole data and age calibrations of seismic units

Drilling sites from ODP Leg 184 (ODP Site 1148), IODP Expeditions 349, 367&368 (U1435, U1499, U1500, U1501, U1502, and U1504) are used to calibrate the age of seismic units. Seismic section N4 lies very close to the IODP Expedition 367&368 drill sites, and therefore the lithologies and ages of both sediments and basement rocks along this section are well constrained by the Sites U1500, U1502 and U1504. Age of the unit boundaries is based on biostratigraphic data (Li et al., 2015; Sun et al., 2018), and the location of unit boundaries in the seismic sections have been estimated converting drilled depth to two-way travel time using P-wave velocities derived from the logging data of relative drilling sites (Fig. 2) (Sun et al., 2018).

The combination of seismic and drill-hole data enabled us to define characteristic seismic units in the Cenozoic infill of the distal northern SCS margin that are interpreted to record distinct tectonic phases. The tectono/seismic units are described hereafter from bottom to top:

The pre-rift unit: mainly identified below Cenozoic grabens in the distal margin and often its top is recognized as the acoustic basement. A distinct angular unconformity (Tg) separates indistinctly the pre-rift or basement from the Cenozoic sediments on top. The internal reflection pattern below Tg is mainly chaotic and
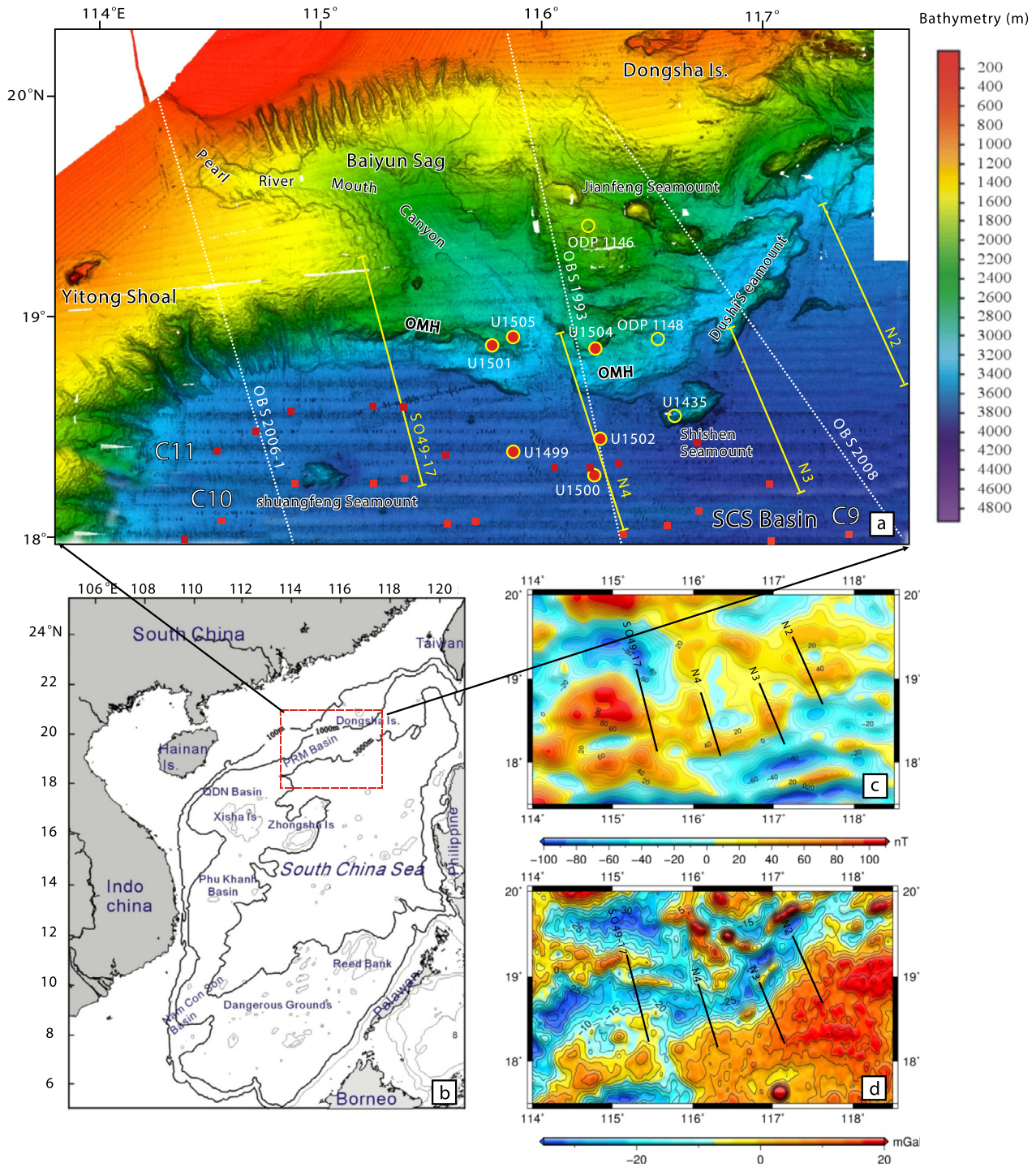
Fig. 1. (a) Morphological features of the middle part of the north continental margin and adjacent regions of the South China Sea. Yellow lines show the locations of example seismic sections discussed in this study. White dashed lines are the wide-angle seismic profiles. Red squares indicate the magnetic lineation from Briais et al. (1993). Drill sites of ODP Leg 184, IODP Expeditions 349, 367&368 are indicated by yellow circles. (b) Major tectonic units and sedimentary basins in the South China Sea. Red dashed square shows the study area. (c) RTP magnetic anomaly map. (d) Free-air gravity anomaly map. (For interpretation of the colors in the figure(s), the reader is referred to the web version of this article.)

discontinuous with various frequency and intensities. Site U1501 located on a broad regional basement high, referred to as Outer Margin High (OMH) (Fig. 1), drilled lithified pre-rift sandstones and conglomerates of uncertain age (Mesozoic?) below an angular unconformity (Sun et al., 2018; Larsen et al., 2018). Site U1504 is located in the eastward prolongation of the OMH, and penetrated a metamorphic basement composed of fine - to coarse-grained epidote-chlorite schists that lie below the Tg level. The exact nature of the protolith as well as its related P-T-t evolution remains unconstrained for the moment (Sun et al., 2018).

Unit 1, or syn-rift unit: deposited before the onset of seafloor spreading ranges from Eocene to Early Oligocene (before ~30 Ma). The acoustic basement (including the *pre-rift unit*) forms the base of this unit. This unit shows subparallel and low to - moderately continuous reflectors with low frequency and various intensities, sealed by a regional unconformity T70 with an age between
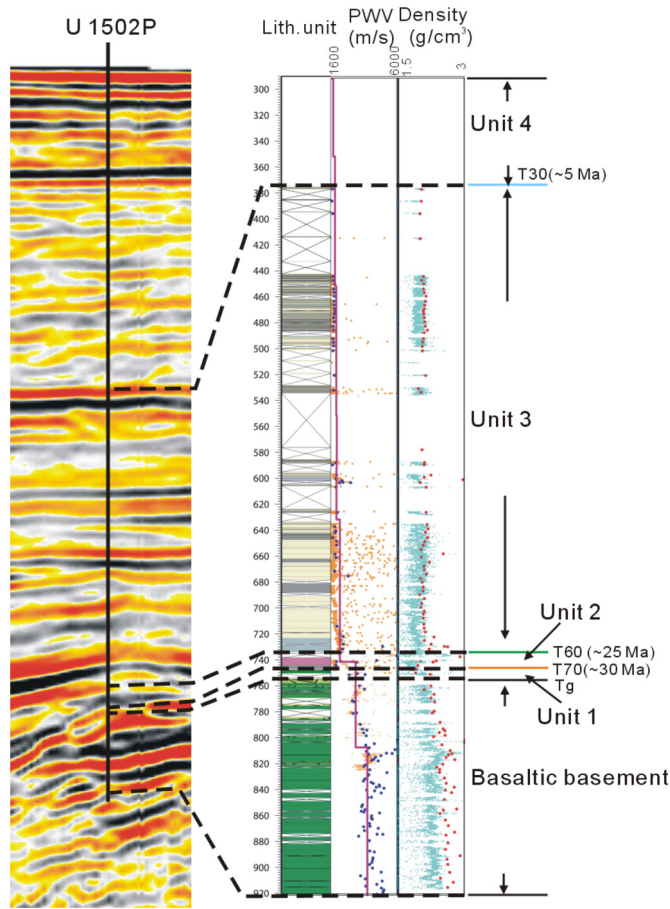
Fig. 2. Calibration of seismic horizons from Site U1502. The interpreted boundaries are calibrated from recovered lithostratigraphy. P-wave velocity and density along the site are shown in depth. Site U1502 has penetrated into basaltic basement and recovered most of the Neogene deposits. See location in Fig. 1.

∼32-30 Ma (Sun et al., 2018). Major thickness variations in the profiles imply that this unit has a syn-tectonic origin. This unit has been penetrated at Site U1501, where it recovered late Eocene siliciclastic sediments presenting a finning upward sequence (Sun et al., 2018). These sediments are similar in age and type to the syn-rift sediments of Site U1435 (Li et al., 2015). A further subdivision of the syn-rift unit sequence was not attempted because of a lack of drill sites in the distal margin. Further oceanward, at Site U1499 on a basement ridge (referred to as Ridge A Fig. 3), an undated gravel unit with silty and sandy intervals has been penetrated (Sun et al., 2018).

Unit 2: deposited since the initial seafloor spreading (∼ 30 Ma) and limited by a regional unconformity T60, which corresponds to a hiatus at ∼23 Ma, sampled at IODP Site U1435 (Li et al., 2015). This hiatus is also present at Sites U1501 and U1502 corresponding to a remarkable lithological change with an age of ∼24 - ∼26 Ma (Sun et al., 2018). In seismic sections T60 can be traced basin-wide by a strong negative phase change. This unit is internally characterized by subparallel to - parallel reflections of high to - intermediate continuity and moderate intensity. The architecture and lithological content of this unit change significantly across the distal margin as a function of topography and related paleowater depth. The representative sedimentary facies of the OMH is found at Sites U1501 and U1505 and is composed of nannofossil rich clay. At Site U1499, above the gravel Unit a condensed section of breccia (from ∼30 to 26 Ma) was drilled. In addition, Site U1502 located on Ridge A eastward of Site U1499 (Figs. 1&5), recovered very hard, poorly sorted breccia and biosiliceous clays (Sun et al., 2018).

Units 3&4: deposited after T60, spanning the early Miocene syn-drift and middle Miocene to present post-drift basin development. These two units have very similar seismic reflectors separated by T30 with an age of ∼ 5 Ma, characterized by parallel reflections with low-to-moderate intensity, locally transparent facies are observed as well. They are made of nannofossil-rich clays, silty clay, foraminifer-rich clayey siltstone to sandstone, and nannofossil oozes deposited in deep marine environments, with minor calcite and chalk (Sun et al., 2018).

3.3. Interpretation of magmatic additions: methodology and terminology

While the combination of drilling results and seismic data enables the determination of sedimentary units that can be correlated across the distal margin, the identification of the amount of magmatic additions related to breakup is challenging and related to large uncertainties (Tugend et al., 2018). In this study, we used seismic criteria, locally supported by drilling results of the IODP expeditions 367&368, to interpret magmatic additions that occur as magmatic sills characterized by spatially limited, high-amplitude reflectors, which can be easily distinguished from the relative low-amplitude, chaotic internal surrounding seismic reflections. (e.g. Trude et al., 2003; Zhao et al., 2016).

### 4. Stratigraphic and tectono-magmatic characteristics of the SCS structural domains

We use four seismic sections imaging the along strike northern SCS margin to document the tectonic and magmatic structures related to breakup. Based on these seismic data combined with geophysical data and drilling results, we tentatively identified different basement types along the margin: the unambiguous thinned continental and oceanic domains. A transitional domain, where the rift-to-drift transition is recorded, occurs in between.

The recognition of these rift domains on reflection seismic data is mainly based on crustal thickness varications, changes in Moho reflectivity, stratigraphic architecture, and top-basement architecture (Figs. 3–6). Magnetic data and the free-air anomaly signals were involved to provide complementary constraints to delimit the spatial extent of these domains on the profiles (see map view in Fig. 1c&d, and along-profile view in Figs. 3–6). These data were collected by the 1:500000 scaling Gravity, Magnetic, and Bathymetric Survey in 2003 to 2007 by the Second Institute of Oceanography, MNR. Variable inclination RTP (reduction-to-the-pole) is employed for the magnetic data.

4.1. Thinned continental domain

Based on seismic observations the thinned continental domain is characterized by: (1) well developed fault bounded basins with thick syn-tectonic sediments; (2) a major reflector around 9-10 s TWT that shallows oceanwards identified as the Moho; and (3) generally negative free-air anomaly, increasing oceanwards to the SE end of this domain. Exception is SO49-17, where the FAA signals change a lot. The crustal thickness ranges from 5.5 to 3 s TWT (16 - ∼7 km), gradually thinning oceanward. The crust in this domain is significantly thinned compared with the ∼30 km thickness of the continental crust documented onshore South China (Braitenberg et al., 2006).

On both N2 and N3 seismic sections, two main basement highs delimit a ∼30 km wide sedimentary basin. The most continentward basement high (between 0 - 15 km in N2, Fig. 3; between 0 - 13 km in N3, Fig. 4) is delimited by several normal faults affecting
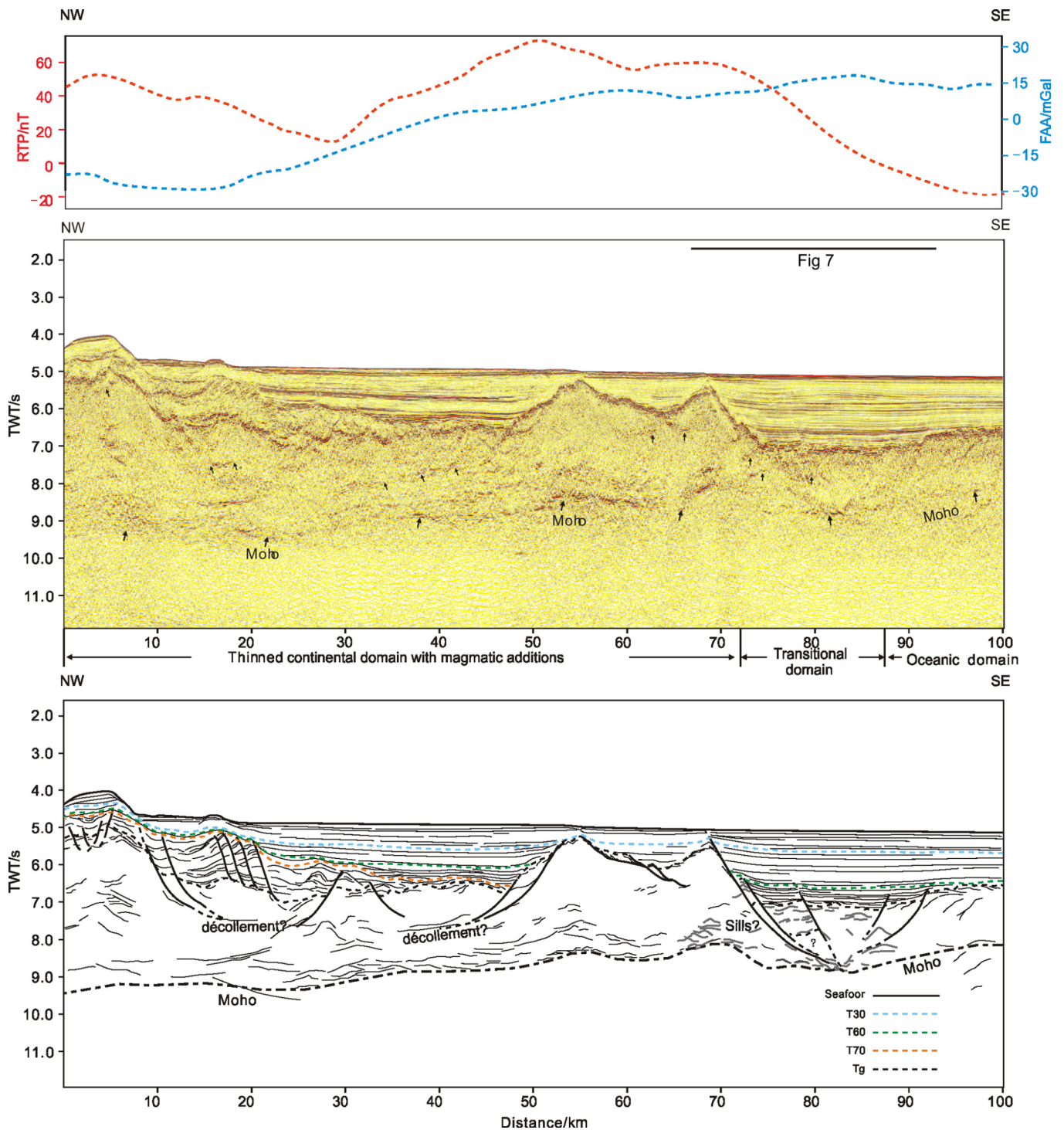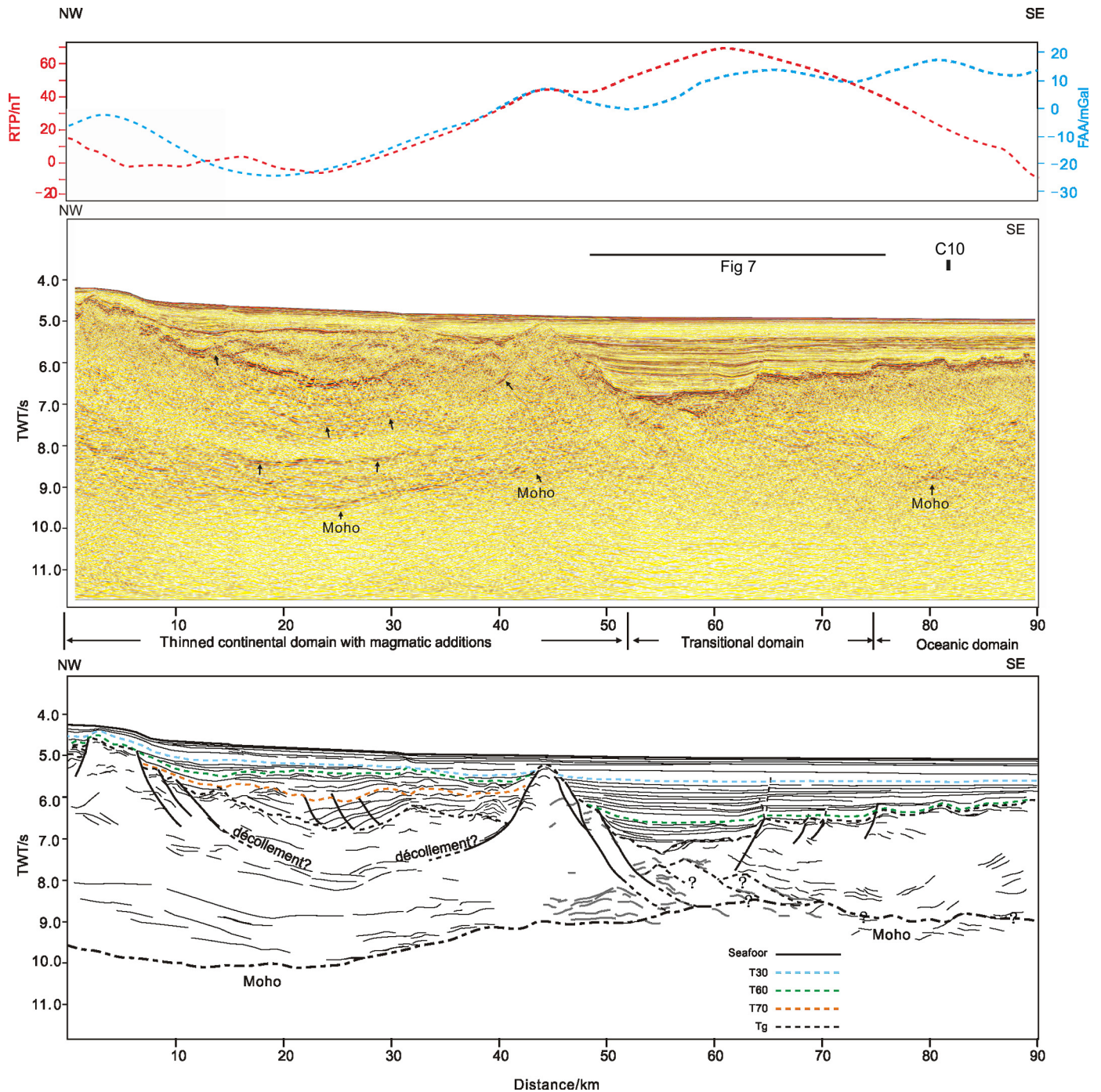
Fig. 3. MCS section N2 in a southeastern direction and the along profile free-air gravity (blue) and RTP magnetic anomaly (red). Middle is the original seismic section. Black arrows indicate strong internal reflectors and Moho; Blow is a geological interpretation with line drawing. Colored dashed lines are the sequence boundaries separating different sedimentary unit. A huge basement high with peak close to the seafloor can be observed in the distal part of the margin, bounded by several listric normal faults. Both the gravity and magnetic anomalies of this basement high increase. Vertical exaggeration is 3.

the continental crust and the overlying syn-rift sediments. These normal faults dip generally toward the ocean. Locally strong horizontal intra-basement reflectors are identified in seismic section N2 (Fig. 3) at 8.0 s TWT. The observed normal faults are consistently soling out in these intra-basement reflectors, showing a typical listric fault shape. Therefore these reflectors at ~8.0 s TWT are interpreted as a major decollement corresponding to the brittle-ductile transition. The *syn-rift Unit 1* shows locally growth structures confirming their deposition during active faulting (Fig. 8).

A basement high (between 45 - 75 km in N2, Fig. 3; 40 – 50 km in N3, Fig. 4) marks the oceanward termination of the thinned continental domain. In seismic sections N2 and N3, the basement high is onlapped on both sides by post-drift sediments while no clear evidence for syn-rift sediments are observed.

Towards the west, this thinned continental domain shows a different architecture. In seismic section N4, a basement high, identified as the OMH (between 20-40 km, Fig. 5), shows a remarkable mound shape with its top being exposed at the seafloor. The OMH

Fig. 4. MCS N3 in a southeastern direction and the along profile free-air gravity (blue) and magnetic anomaly (red). Middle: Original seismic section; Blow: a geological interpretation with line drawing. Colored dashed lines are the sequence boundaries separating different sedimentary unit. A basement high separates the continental domain from the transitional domain. Two oceanward dipping listric faults (solid black line) bounds the SE side of this basement high and soles out in the Moho. Vertical exaggeration is 3.

was drilled at three locations (Sites U1504, U1501 and U1505). Two Sites were able to penetrate the *pre-rift unit/acoustic basement*. Site U1504 lies very close (∼10 km) to the east of the section N4, recovering fine - to coarse-grained epidote-chlorite schist with unknown age (Sun et al., 2018). In Site U1501, located further to the SW, the *pre-rift Unit/acoustic basement* is composed of well lithified sandstones interbedded with siltstones and conglomerates, containing magmatic clasts possibly of Mesozoic age (Sun et al., 2018; Larsen et al., 2018).

On the NW side of the OMH, a thick sedimentary package (1.2∼1.7 s TWT) is observed that connects with the southern part

of the PRMB towards the NW. In this area, the top of the *pre-rift unit/acoustic basement* is marked by a continuous strong reflector without evidence for significant normal faulting. This OMH is delimited by two oceanward-dipping normal faults in the SE side.

Seismic section SO49-17 lies in the westernmost part of the study area (Figs. 1, 6). To the NW (between 0 - 40 km, Fig. 6), the acoustic basement documents contrasted topographies related to both landward and oceanward-dipping normal faults. These extensional structures controlled the formation of rift basins associated with wedge-shaped geometries belonging to the *syn-rift unit 1*. Local intra-basement reflectors are identified at about 6.5 s TWT,
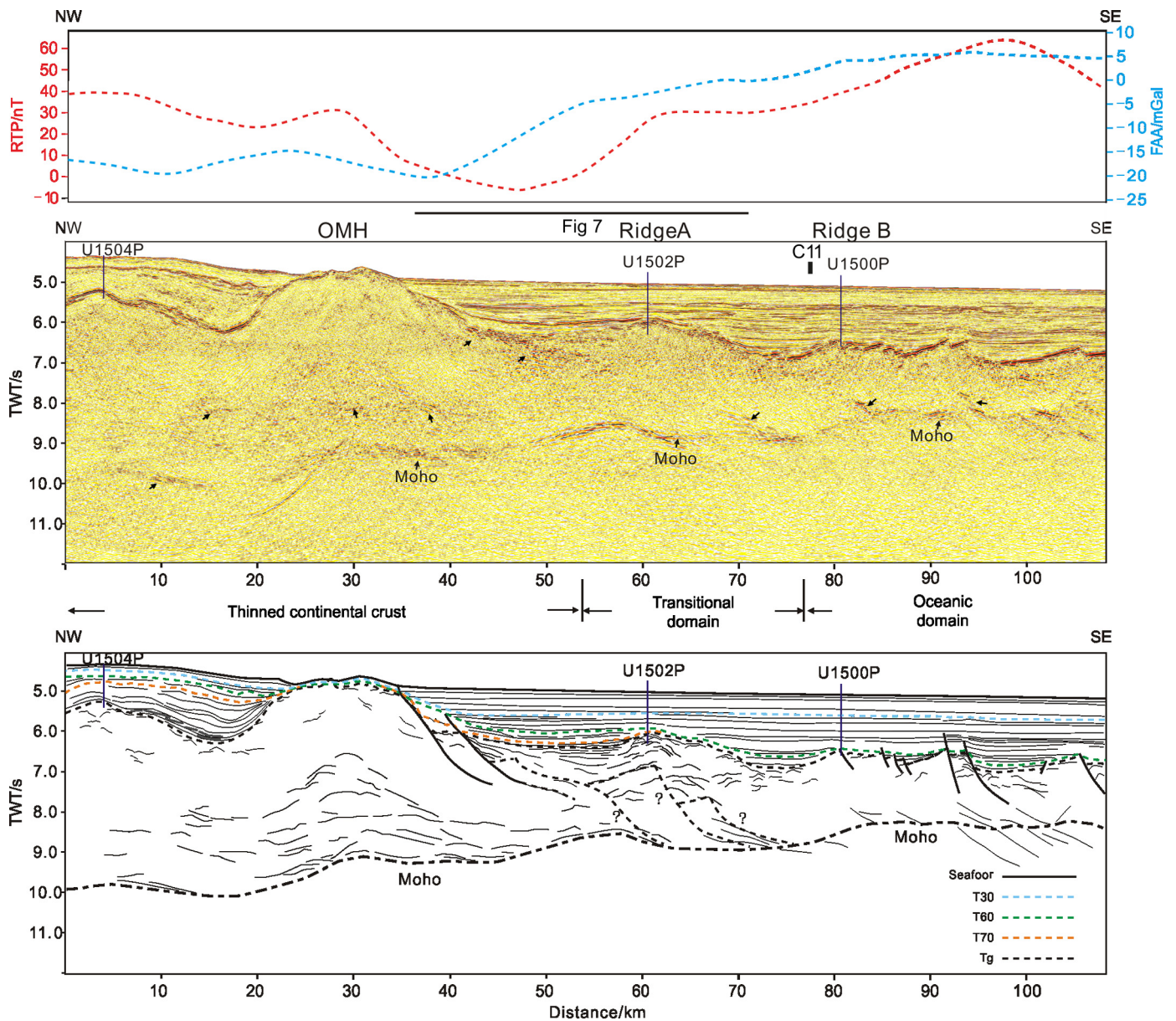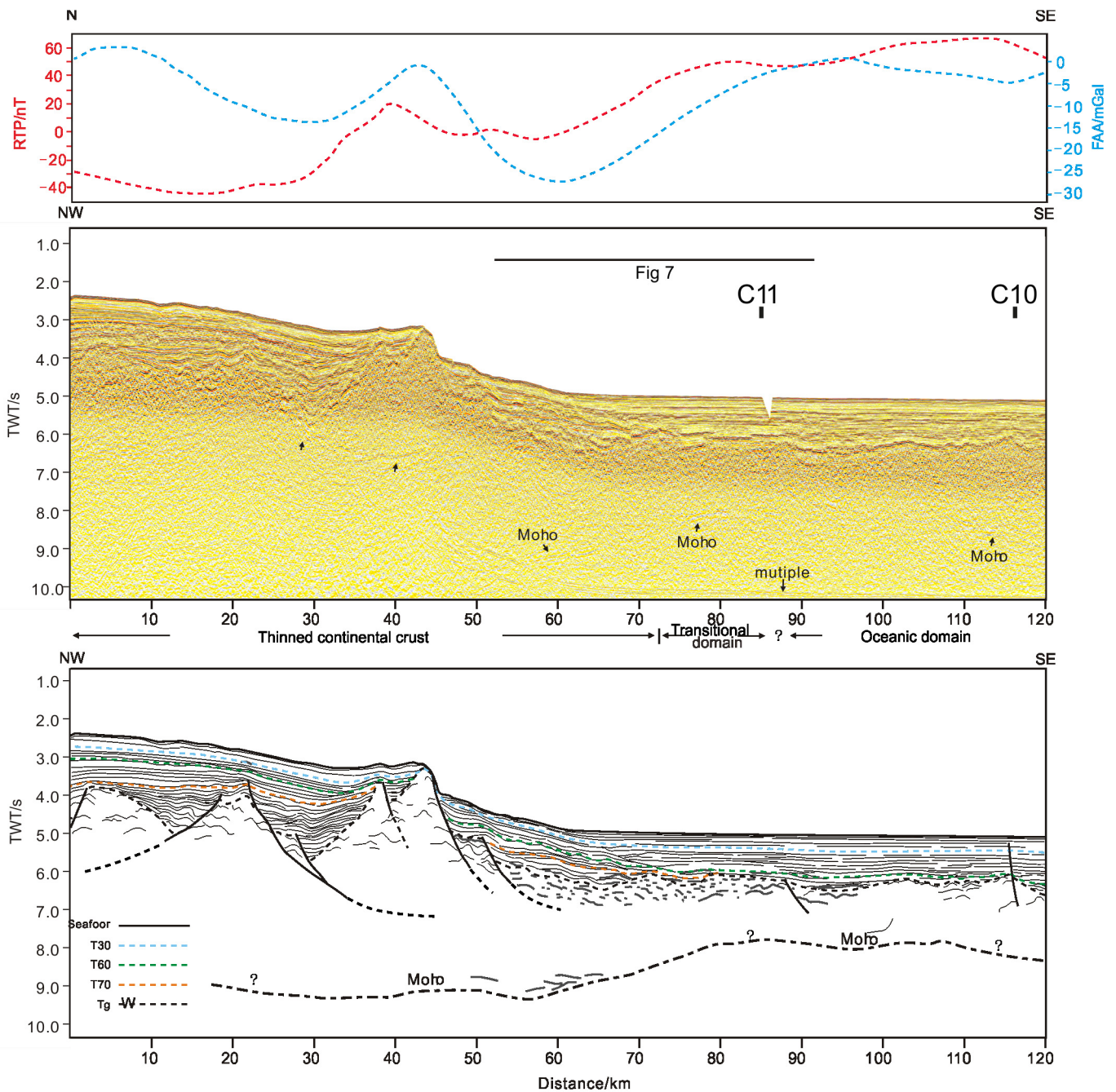
Fig. 5. MCS section N4 in a southeastern direction and the along profile free-air gravity (blue) and magnetic anomaly (red). Middle: Original seismic section; Below: a geological interpretation with line drawing. Locations of Sites U1502 and U1500 are projected along the line. Colored dashed lines are the sequence boundaries separating different sedimentary unit. A basement high (referred as Outer Margin High, OMH) with a mound shape can be observed drilled at Site U1504P, with the top piercing the seafloor. Several strong internal reflectors are interpreted as oceanward dipping listric normal faults (dashed black line) developed within the Ridge A in the distal margin. Ridge A is penetrated at U1502P. Further oceanward is the Ridge B of basaltic basement, drilled by U1500P. Vertical exaggeration is 3.

possible corresponding to the depth of the décollement level of listric faults characterizing the thinned continental domain. Similar to the other profiles, the end of the thinned continental domain is marked by a continental high (between 30 - 50 km, Fig. 6) that shows quite high gravity and magnetic signals (Fig. 1a, c&d). Two oceanward-dipping normal faults can be identified in the SE side of this basement high, which are associated with several steps of the top of the acoustic basement. The crustal thickness decreases gradually with the Moho shallowing up from ∼ 9 s to ∼8 s TWT. The basement is rugged and overlain by wavy syn-rift Unit 1 with varying thickness. This unit extends oceanward to about the edge of a basement high.

Only little evidence for magmatic activity is interpreted in the thinned continental domain. Discontinuous sub-horizontal strong reflectors within the sedimentary packages present a saucer- or bowl-shaped geometry characteristic of magmatic sills (seismic section N4 between 15 - 20 km, Fig. 5). Local discontinuous reflec-

tive packages above the Moho could correspond to intrusive dikes in the lower crust, notably towards the oceanward end of the domain (Fig. 3–6). Two wide-angle seismic profiles (OBS2008 (Chiu, 2010) and OBS1993 (Yan et al., 2001)), which lie between the seismic sections N2-N3 and N3-N4 respectively (Fig. 1) indicate that the lower crust below the continental slope corresponds to a high velocity layer (HVL) interpreted as related to magmatic mafic underplating.

However, the determination of the timing of magmatic addition emplacement is challenging notably within basement and some are likely to predate continental breakup. In addition, the lateral repartition of these potential mafic underplating is likely variable as suggested by the lack of evidence for a HVL in the wide-angle seismic profile OBS2006-1 lying in the west (Fig. 1, Ding et al., 2011). The low resolution of both the gravity and magnetic signals provides limited constraints given the small amount of magmatic additions that can be interpreted. Still, they do not support the

Fig. 6. MCS section SO49-17 in a southeastern direction and the along profile free-air gravity (blue) and magnetic anomaly (red). Middle: Original seismic section; Below: a geological interpretation with line drawing. Colored dashed lines are the sequence boundaries separating different sedimentary unit. A basement high separates the abyssal basin and the continental slope. Fragmentary, but occasionally strong internal reflectors can be identified below this basement high. Vertical exaggeration is 3.

occurrence of large magmatic intrusions along the profiles investigated.

4.2. Transitional domain

The transitional domain along the four seismic sections represents a ~15 ~ 25 km wide area between the continental and the oceanic domains. This domain is characterized by (1) an irregular crustal thickness ranging from 1.2 to 1.8 s TWT (~7 km to 11 km); and (2) complex and chaotic intra-basement high-amplitude reflectors (Fig. 8). Evidence of magmatic additions is more frequent in this domain than in the thinned continental one and they seem to be controlled by tectonic activity.

The transitional domain in seismic section N2 starts at the southeastward edge of the basement high (Fig. 7a). This edge is characterized by an oceanward dipping listric fault rooting deeper than in the thinned continental domain, possibly near the interpreted Moho. The top basement of the transitional domain lies at ~7 s TWT and appears faulted. Several strong amplitude reflections are observed within the basement above the Moho at 9 s TWT (between 68 – 84 km, Figs. 3&7a). Some of them have bowl shape with sharp edges and could correspond to dykes intruded in the lower crust. We propose that the footwall of the major listric normal fault is composed of thinned continental crust with magmatic additions, whereas the hanging wall is interpreted as volcanoclastic material (including sediments and basaltic flows) possibly resting on remnants of continental crust. The lower part
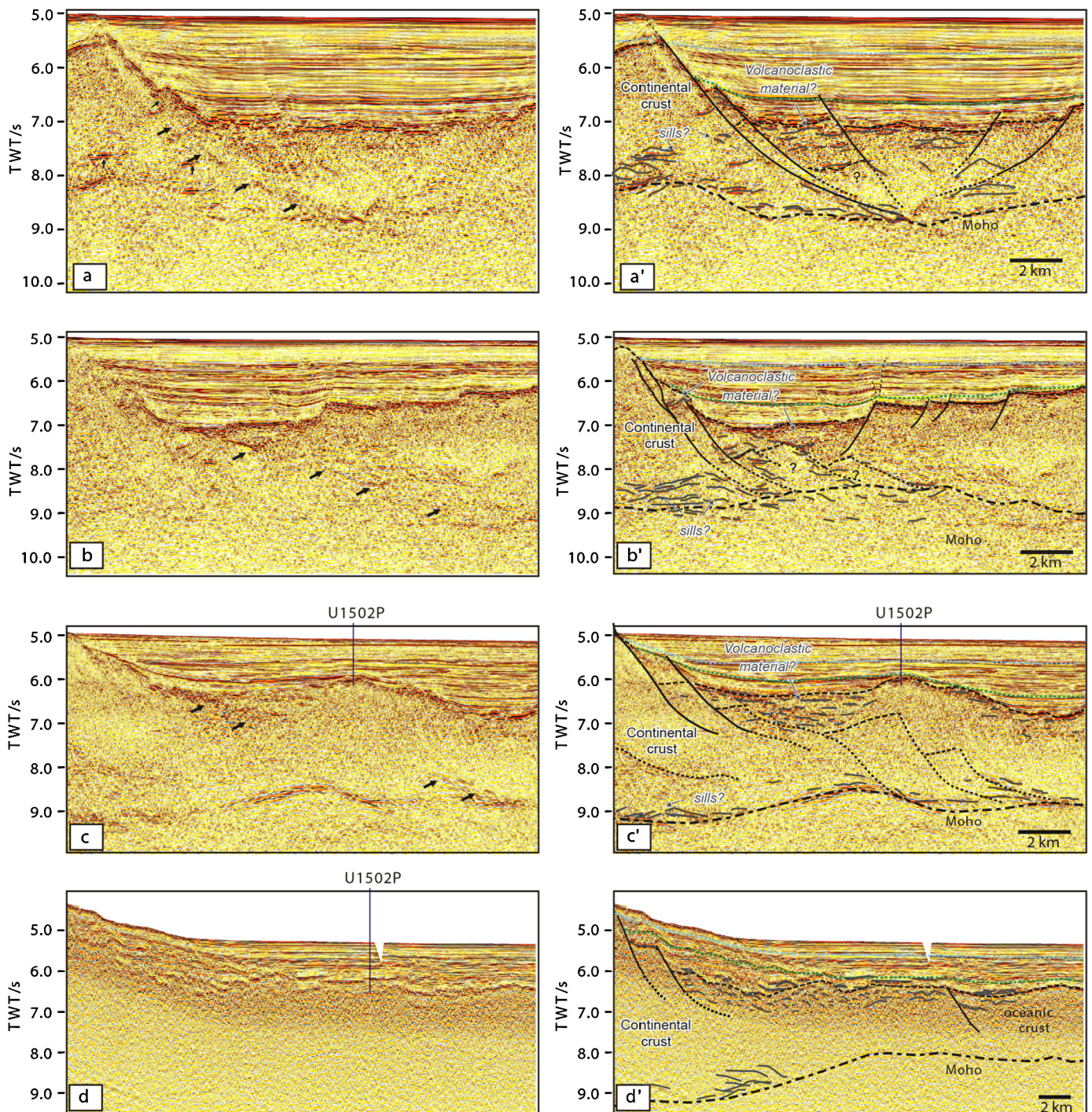
Fig. 7. Enlarged original (left) and interpreted (right) sections display expanded view of the transitional domain. Fig. 7a from N2, Fig. 7b from N3, Fig. 7c from N4, and Fig. 7d from SO49-17, respectively.

of the *Unit 2* (Tg-T60) presents growth structures onlapping on the major fault and sealed by undeformed sediments.

In seismic section N3, the architecture of the transitional domain is very similar with that of N2. Two oceanward dipping normal faults board the NE part with stepped-down basement possibly rooting near the Moho at ∼9 s TWT (Fig. 7b). These faults seem to separate different types of acoustic basement, showing different seismic facies. The footwall is characterized by low - to medium amplitude, discontinuous reflectors which are similar with those of the thinned continental crust in the northwest. Strong internal reflectors exist within the basement above the Moho (between 45 - 55 km, Figs. 4&7b). We interpret these light reflectors as mag-

matic dykes in the lower crust. The top basement on the hanging wall side shows medium to - strong amplitude, sub-continuous reflectors, overlain by very strong amplitude reflectors on the top (basaltic flows?). The sediments of *Unit 2* are undeformed and unaffected by magmatism which implies a short interval of magmatism at breakup.

The transitional domain in seismic section N4 is separated from the continental domain by the Ridge A (Fig. 7c). Disconnected strong oceanward dipping reflectors can be identified within the basement. We interpreted them as markers of listric normal faults possibly rooting near Moho between 8 - 9 s TWT. The basement of the hanging wall is characterized by strong to medium am-
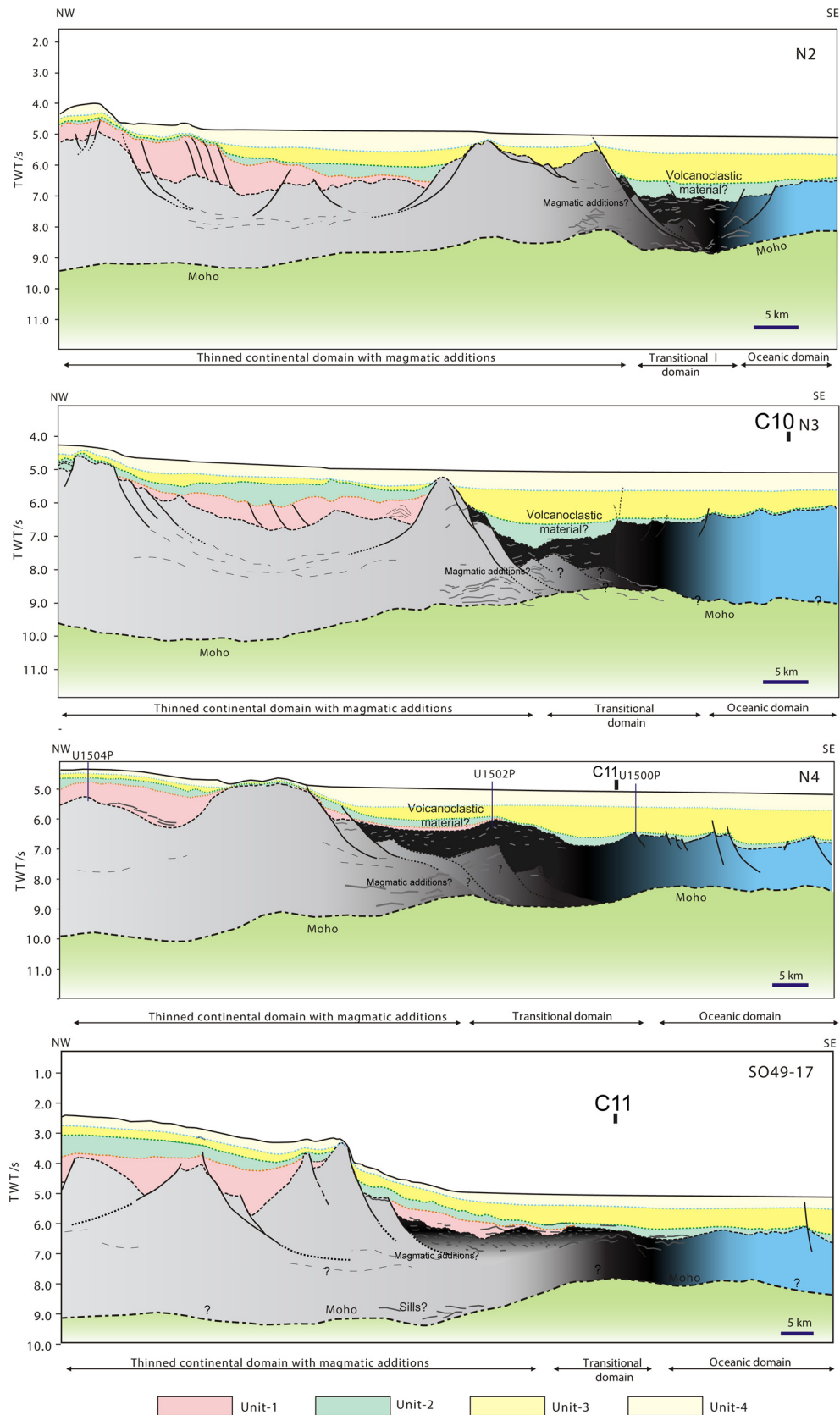
Fig. 8. Gathered geological interpretations of all four seismic sections from east to west. Three basement domains are identified, including the thinned continental crust with magmatic additions; the transitional domain, and the oceanic domain with slight normal faults. The thinned continental crust thins toward the oceanic basin with thickness between 7 and 16 km, and is dominated normal faulting with syn-tectonic sediments. The transitional domain is narrow (<20 km) and dominated by hyper-extended crust complicated by magmatic intrusion, indicating a rapid rift-to-drift transition and interaction between tectonics and magmatic processes. The oceanic domain is steady-state oceanic crust with slight normal faulting.

plitude, sub-continuous, parallel to sub-parallel reflectors. Drilling results at Site U1502 locating a few km east of the line on this ridge present altered basaltic breccia, brecciated basalts and altered pillow basalts (Sun et al., 2018), confirming magmatic activity. Different types of veins, including composite silica-rich veins, composite epidote-rich veins and composite carbonate veins crosscut the basalts and indicate intense hydrothermal circulation. Clay to claystone was cored immediately above basaltic basement with an assemblage of agglutinated benthic foraminifera, indicating a late Eocene age (Sun et al., 2018). Site U1499, which is ∼40 km west of Site 1502 along Ridge A, ended below Tg in undated gravel. The last age datum comes from matrix-supported breccia deposited between 30 to 26 Ma (Sun et al., 2018). All these drilling results prove that the Ridge A was formed before the initial seafloor spreading. The *syn-rift unit 1 is* deposited right above the basement between the OMH and Ridge A, and is overlain by Units 3, 4&5 with horizontal, parallel reflections. Transparent and coherent patterns are observed in the footwall of the normal faults and are interpreted to consist of rotated continental blocks. Some strong internal reflectors exist within the basement above the Moho (between 55 – 70 km, Figs. 5&7c), possibly indicating magma intrusions. As emphasized by Larsen et al. (2018), the Moho can be followed from the thinned continental crust until the oceanward edge of Ridge A sampled by the Site U1502 on the section N4. This suggests that first magmatic additions were emplaced over and within thinned continental crust.

The transitional domain in seismic section SO49-17 is defined as a ∼ 15 km-wide segment between the thinned continental and the oceanic domains (Figs. 6, 7d), characterized by a highly reflective top and shallowest Moho depth (∼8 s TWT). No obvious normal fault has been identified within the basement. The deposits above are un-deformed feature with parallel to sub-parallel, continuous reflectors.

4.3. Oceanic domain

Along the four seismic sections (Fig. 8) the following features characterize the architecture of the oceanic domain: (1) the base of the crust is clearly marked by a set of moderate to high continuity reflections, interpreted as oceanic Moho located between 8-9 s TWT. (2) the top of igneous basement is characterized by high-amplitude, subhorizontal and continuous reflections; (3) The crustal thickness varies from 1.8 to 2.8 s TWT, but ranges mostly between 1.8 and 2.2 s TWT; and (4) The appearance of oceanic magnetic anomalies on the profiles (Magnetic anomaly C10 on N3, Fig. 4; C11 on N4, Fig. 5; and C11, C10 on SO49-17, Fig. 6). In addition, using wide angle velocities (Chiu, 2010), the oceanic crustal thickness was inferred to range between 5.4 and 8.4 km, and the top basement morphology is not entirely flat and smooth, but complicated by a set of faults and tilted blocks. In seismic section N4, the acoustic basement is clearly offset by several oceanward normal faults, forming several isolated basins (Fig. 5). The lower part of the *Unit 2* appears to be syn-tectonic, forming growth structures with thickness variation. The upper part of the *Unit 2*, and of *Units 3&4* are generally not perturbed by deformation and seals the fault-bounded tilted blocks.

This domain was drilled during IODP expeditions 367&368. The Site U1500 is located close to the seismic section N4 and sampled the edge of Ridge B. IODP Site U1500 cored ∼115 m basaltic basement with a recovery of 77%. Shipboard petrological studies showed that the basalts have a classical MORB composition similar to the basalts sampled on the central part of the SCS oceanic domain during the IODP Expedition 349 (Li et al., 2015; Sun et al., 2018). These basalts are overlain by post-drift sediments made of deep marine clay, claystone, sandstone with silt and sandy silt intervals.

5. Discussion

5.1. Architecture of the COT and lateral variability

Some along-strike similarities can be found in the architecture of the transitional domain shown in this work. The thinned continental domain is generally terminated by a basement high separated from the transitional domain by one or two major listric normal fault(s) rooting near the interpreted Moho. Oceanward of the major listric fault(s), the upper part of the basement is reflective, locally showing growth sequences towards the fault (seismic sections N2&N3), possibly corresponding to volcano-clastic material. The smoother and highly reflective top basement towards the oceanic domain might indicate basaltic flow, which has been penetrated by Site U1502. Below this sequence, we suggest the occurrence of pieces of continental remnants. We thus interpret this domain as an igneous crust with possible variable remnants of continental crust. The hybrid type of crust of the transitional domain is interpreted to record the rift-to-drift transition. Referred to as transitional domain in this work (using the same terminology as Welford et al., 2010) (Fig. 8), it compares to the 'embryonic oceanic crust' (Jagoutz et al., 2007), 'proto-oceanic' (Gillard et al., 2015; Tugend et al., 2018) or 'outer domain' (Péron-Pinvidic et al., 2007) described at other rifted margins.

A lateral variability of the COT architecture nevertheless occurs along strike. In the E part as shown in seismic sections N2 and N3 (Fig. 8), the transitional domain shows very similar architectures featured with abrupt changes from thinned continental domain with listric normal fault(s), extremely thinned continental blocks in the lower part covered by possible volcanoclastic materials. The lower part of the sedimentary succession is controlled by normal faults. While further to the W, the equivalent of Ridge A is thicker than in the seismic sections N2 and N3, possible related with thicker continental crust remnant and intensive magmatic activities.

The transitional domain of the SO49-17 lying in the westernmost part shows some differences. No obvious normal faults were observed (this could be due to the lower resolution) and the width is narrower (∼ 15 km compared with ∼15 - ∼25 km of the above three sections in the east) (Fig. 8). Magmatic additions appear more limited, and no HVL is evidenced beneath the lower crust. Cameselle et al. (2017) suggested that the narrow character of this transitional domain was due to an abrupt thinning of the continental lithosphere in the Northwest Sub-basin (NWSB). A transform fault termed as Zhongnan Fracture zone has been reported, which separates the NWSB from the ESB, delimiting a change in the depth of acoustic basement (e.g., Li et al., 2015; Cameselle et al., 2017; Larsen et al., 2018) and may also mark the change in the architecture of the transitional domain.

5.2. Tectono-magmatic evolution of the rift-to-drift transition at the SCS

Rifting at the SCS margin appears at first order as a symmetric process, strongly controlled by the occurrence of a weak lower crust (Franke et al., 2014; Brune et al., 2017). Polyphase extension was mainly controlled by a major décollement located between the brittle upper crust and ductile lower crust (brittle-ductile transition), interpreted to form intra-basement shear zones acting as the main crustal thinning mechanism (Franke et al., 2014; Gao et al., 2015; Zhao et al., 2018). In addition to this main décollement, additional shallower décollement levels can be interpreted on seismic sections (Fig. 8), controlling the variability in the structural style observed in the thinned continental domain. The occurrence of several décollements at various depths is also reported based on high quality seismic data in the Dangerous

Ground area (e.g. Ding et al., 2013; Liang et al., 2019), highlighting along strike variations of the architecture of the SCS margins. However, they all image listric normal faults soling out in lower crustal levels and minor high-angle normal faults showing only little offset (Fig. 8). This high-angle type faults cannot accommodate a lot of extension suggesting that normal faulting in the brittle upper crust cannot be the only mechanism that thinned the continental crust. The presence of a weak lower crust at the onset of the SCS rifting might have triggered a ductile necking of the lower crust within intra-basement shear zones interpreted as the main crustal thinning mechanism (e.g. Clift and Lin, 2001; Franke et al., 2014; Zhao et al., 2018). Crustal thinning at the SCS was therefore controlled by a non-uniform extensional mode resulting from an important partitioning of extensional deformation between the brittle upper crust and a weak ductile lower crust.

Studies on major and trace elements of Eocene volcanic rocks from petroleum drill hole samples in the PRMB indicate the local occurrence of basaltic rocks emplaced during rifting (Zou et al., 1995). They appear limited in time and space (Gao et al., 2015).

The distal margin records the latest rifting stage of the northern SCS during late Eocene (Larsen et al., 2018). Extension likely remained symmetric, accommodated by pure shear extension until progressive coupling between crustal and mantle deformation triggered breakup (Brune et al., 2014). This coupling between upper crustal and mantle deformation may be explained by the extreme thinning of ductile lower crustal levels enabling a crustal embrittlement enhanced by crustal cooling during thinning. Faults that cut the entire residual crust and rooted near the Moho are interpreted as structuring the edge of the extremely thinned continental crust (locally less than 10 km thick). Oceanward, in the transitional domain, magmatic additions become dominant (Fig. 8).

The transitional domain seems characterized by the emplacement of extrusive basalts on top of the hyper-extended continental crust (MORB-type magmatism drilled at Sites U1500 and U1502), intrusive dykes in the lower continental crust.

Based on these interpretations, we suggested that continental breakup along the central northern SCS occurred rapidly during the latest stage of rifting, and magma potentially used fault systems of the distal margin to percolate and inject through the hyper-thinned continental crust as exemplified at Site U1502 were a volcanic edifice built over a fault block. The transitional domain of the SCS margin seems characterized by a progressive increase of magmatism in time and space from latest rifting to breakup, overprinting the hyper-thinned continental crust. Breakup likely occurred rapidly in continuum with the crustal and lithospheric thinning that triggered decompression melting. This magmatic event might also contribute to the formation of the HVL beneath the middle and east part of the continental slope.

5.3. Implications for the interpretation of the SCS margin type

Considering the apparent reasonable amount of magmatic supply during rifting, the absence of exhumed mantle or SDRs in the transitional domain, the SCS does not seem to fit into classical end-member magmatic archetypes. Instead, the SCS margin appears 'intermediate' in term of magmatic volumes at breakup. Instead of considering magmatic volumes, rifted margins may also be considered based on the relative timing of decompression melting and melt extraction relative to the amount of crustal thinning (Tugend et al., 2018). Interestingly, magma-poor systems, such as the Iberia-Newfoundland continental margins, are characterized by a delay in decompression melting and melt extraction that post-dates lithospheric breakup (e.g. Péron-Pinvidic et al., 2007; Brune et al., 2017; Tugend et al., 2018). This enables the formation of several tens to hundreds of kilometers wide zones of exhumed subcontinental mantle potentially experiencing long-duration tectonism and

multi-stage stuttering magmatic activity (Sutra et al., 2013). In contrast, magma-rich systems show an early onset of magmatic production and emplacement relative to crustal separation. Extreme crustal and lithospheric thinning of the SCS margin likely triggered a rapid onset decompression melting of the ascending asthenosphere.

5.4. Origin of syn-breakup magmatism

The parameters controlling the onset of magmatic activity and magmatic supply at breakup are numerous. These include the mantle temperature (e.g. Nielsen and Hopper, 2004), the upwelling rate of asthenosphere (e.g. Forsyth, 1992), the inherited extension history before seafloor spreading (e.g. Minshull et al., 2001), and possible the sedimentary insulation (e.g. Lizaralde et al., 2007). An anomalously low mantle temperature will suppress melting at the time of continental breakup. These "cool" mantle spots are rare and existed under some typical magma-poor margins, such as the Australian-Antarctic margin (Cochran et al., 1997) and West Iberia margin (Minshull et al., 2001). Regions of anomalously high mantle temperature appear commonly associated to magma-rich margins (e.g. Skogseid, 2001). Clift and Lin (2001) suggested the presence of a significant positive mantle thermal anomaly in the northern continental margin of the SCS at the time of breakup based on the calculation of the total amount of subsidence. Other studies also confirmed anomalously hot thermal condition of the continental lithosphere at the time of extension, implying that the continental crust was thermally weakened (Clift, 2015).

We suggest that magmatic additions in the transitional domain mainly originated from decompression melting of the ascending asthenosphere resulting in typical MORB signatures, as confirmed by preliminary geochemical data on Sites U1502 and U1500 (Larsen et al., 2018). Fast extension in the SCS margin eventually leading to continental breakup, seems like a key factor that enhanced the magmatic production (Larsen et al., 2018). Extension appears to have started in the Eocene (Briais et al., 1993; Brune et al., 2017), as also evidenced from the Site U1501. In this site, the last age datum is at 34 Ma, recorded at 200 m above the base of the syn-rift sequence. Based on this dataset, Larsen et al., 2018 inferred a late Eocene age for the oldest sediments lying just above acoustic basement. Thus, the main rift event that preceded breakup lasted less than 10 Myrs. This rapid extension would have favored the upwelling of hot material, with a minimal cooling effect. This may explain the generation of enhanced and localized magma during breakup.

Future geochemical studies on the cored basaltic rocks from IODP Sites U1500 and U1502 could provide more detailed information about the type of mantle that is at the origin of the magma, the mantle temperature and degree of depletion.

6. Conclusions

Thanks to high quality seismic data and benefiting from the IODP Expeditions 367&368 that drilled across the COT, the northern South China Sea margin represents a critical natural laboratory to study the processes and parameters controlling the rift-to-drift transition. Three types of basement domains have been identified based on the basement architecture and its interpreted nature, i.e. *thinned continental domain* with typical extensional structures, *transitional domain* where rift-to-drift processes are recorded, and the *oceanic domain*.

Preliminary drilling results in the rift-to-drift transition zone cored MOR-type basaltic basement with no evidence of exhumed mantle, implying a remarkable difference with the end-member magma-poor continental margin model. Seismic interpretations

suggest that this transition is narrow and characterized by a complex basement structure, including remnants of hyper-thinned continental crust overprinted by extrusive and intrusive magmatic material. We suggest that the formation of this hybrid basement is best explained by a magmatic event that occurred rapidly during the latest stage of rifting to trigger continental breakup, followed by steady-state seafloor spreading.

Considering the limited magma additions during rifting and the absence of exhumed mantle or SDRs, the SCS does not seem fit into the classical end-member magmatic archetypes. Instead, regarding the magmatic volumes at breakup, the SCS margin appears 'intermediate'. Breakup occurred after the crustal and lithospheric thinning would have triggered the decompression melting onset of the ascending asthenosphere, and the following seafloor spreading.

Declaration of competing interest

The authors declare that they have no known competing financial interests or personal relationships that could have appeared to influence the work reported in this paper.

Acknowledgement

References

Abdelmalak, M.M., Andersen, T.B., Planke, S., Faleide, J.I., Corfu, F., Tegner, C., Shephard, G.E., Zastrozhnov, D., Myklebust, R., 2015. The ocean-continent transition in the mid-Norwegian margin: insight from seismic data and an onshore Caledonian field analogue. Geology 43, 1011–1014.

Barckhausen, U., Engels, M., Franke, D., Ladage, S., Pubellier, M., 2014. Evolution of the South China Sea: revised ages for breakup and seafloor spreading. Mar. Pet. Geol. 54 (B), 599–611. https://doi.org/10.1016/j.marpetgeo.2014.02.022.

Boillot, G., Grimaud, S., Mauffret, A., Mougenot, D., Kornprobst, J., Mergoil-Daniel, J., 1980. Ocean-continent boundary off the Iberian margin: a serpentinite diapir west of the Galicia Bank. Earth Planet. Sci. Lett. 48 (1), 23–34. https://doi.org/10.1016/0012-821X(80)90166-1.

Braitenberg, C., Wienecke, S., Wang, Y., 2006. Basement structures from satellite-derived gravity field: South China Sea ridge. J. Geophys. Res. 111, B05407. https://doi.org/10.1029/2005JB003938.

Briais, A., Patriat, P., Tapponnier, P., 1993. Updated interpretation of magnetic anomalies and seafloor spreading stages in the South China Sea: implications for the Tertiary tectonics of Southeast Asia. J. Geophys. Res. 98 (B4), 6299–6328.

Brune, S., Heine, C., Pérez-Gussinyeé, M., Sobolev, S.V., 2014. Rift migration explains continental margin asymmetry and crustal hyper-extension. Nat. Commun. 5, 4014. https://doi.org/10.1038/ncomms5014.

Brune, S., Heine, C., Clift, P.D., Perez-Gussinye, M., 2017. Rifted margin architecture and crustal rheology: reviewing Iberia-Newoundland Central South Atlantic and South China Sea. Mar. Pet. Geol. 79, 257–281.

Cameselle, A.J., Ranero, C.R., Franke, D., Barckhausen, U., 2017. The continent-ocean transition on the northwestern South China Sea. Basin Res. 29 (S1), 73–95.

Chiu, M., 2010. The p-Wave Velocity Modeling of the Transitional Crust in the Northern South China Sea Continental Margin. Natl. Taiwan Ocean. Univ., Keelung.

Clift, P.D., 2015. Coupled onshore erosion and offshore sediment loading as causes of lower crust flow on the margins of South China Sea. Geosci. Lett. 2 (1), 1–11. https://doi.org/10.1186/s40562-015-0029-9.

Clift, P.D., Lin, J., 2001. Preferential mantle lithospheric extension under the South China margin. Mar. Pet. Geol. 18 (8), 929–945. https://doi.org/10.1016/S0264-8172(01)00037-X.

Cochran, J.R., Sempere, J.C., SEIR Scientific Team, 1997. The Southeast Indian Ridge between 88oE and 118oE: gravity anomalies and crustal accretion at intermediate spreading rates. J. Geophys. Res. 102, 15463–15487.

Cullen, A., Reemst, P., Henstra, G., Gozzard, S., Anandaroop, R., 2010. Rifting of the South China Sea: new perspective. Pet. Geosci. 16, 273–282.

Ding, W.W., Franke, D., Li, J., Steuer, S., 2013. Seismic stratigraphy and tectonic structure from a composite multi-channel seismic profile across the entire Dangerous Grounds, South China Sea. Tectonophysics 582, 162–176.

Ding, W.W., Schnabel, M., Franke, D., Ruan, A.G., Wu, Z.L., 2011. Crustal structure across the northwestern margin of South China Sea: evidence for magma-poor rifting from a wide-angle seismic profile. Acta Geol. Sin. 86 (4), 854–866.

Ding, W.W., Sun, Z., Dadd, K., Fang, Y., Li, J., 2018. Structures within the oceanic crust of the central South China Sea basin and their implications for oceanic accretionary processes. Earth Planet. Sci. Lett. 488, 115–125.

Fan, C., Xia, S., Zhao, F., Sun, J., Cao, J., Xu, H., Wan, K., 2017. New insights into the magmatism in the northern margin of the South China Sea: spatial features and volume of intraplate seamounts. Geochem. Geophys. Geosyst. https://doi.org/10.1002/2016GC006792.

Forsyth, D.W., 1992. Geophysical constraints on mantle flow and melt generation beneath mid-ocean ridge. In: Morgan, J.P., Blackman, D.K., Sinton, J.M. (Eds.), Mantle Flow and Melt Generation at Mid-Ocean Ridges. In: Geophysical Monographs, vol. 71. American Geophysical Union, pp. 1–65.

Franke, D., Ladage, S., Schnabel, M., Schreckenbergen, B., Reichert, C., Hinz, K., Paterlini, M., Abelleyra, J., Siciliano, M., 2010. Birth of a volcanic margin off Argentina, South Atlantic. Geochem. Geophys. Geosyst. 11 (2), 1–20.

Franke, D., Savva, D., Pubellier, M., Steuer, S., Mouly, B., Auxietre, J., Meresse, F., 2014. The final rifting evolution in the South China Sea. Mar. Pet. Geol. 58B, 704–720.

Gao, J., Wu, S., McIntosh, K., Mi, L., Yao, B., Chen, Z., Jia, L., 2015. The continent-ocean transition at the mid-northern margin of the South China Sea. Tectonophysics 654, 1–19.

Gillard, M., Autin, J., Manatschal, G., Sauter, D., Munschy, M., Schaming, M., 2015. Tectonomagmatic evolution of the final stages of rifting along the deep conjugate Australian-Antarctic magmapoor rifted margins: constraints from seismic observations. Tectonics 34, 2015TC003850.

Jagoutz, O., Muntener, O., Manatschal, G., Rubatto, D., Peron-Pinvidic, G., Turrin, B.D., Villa, I.G., 2007. The rift-to-drift transition in the North Atlantic: a stuttering start of the MORB machine? Geology 35 (12), 1087–1090.

Koppers, A., 2014. On the $^{39}Ar/^{40}Ar$ dating of low-potassium ocean crust basalt from IODP expedition 349, South China Sea. In: 2014 AGU Fall Meeting. T31E-03.

Larsen, H.C., Saunders, A.D., 1998. Proceedings of the Ocean Drilling Program. Scientific Results (Ocean Drilling Program), vol. 152.

Larsen, H.C., Mohn, G., Nirrengarten, M., et al., 2018. Rapid transition from continental breakup to igneous oceanic crust in the South China Sea. Nat. Geosci. https://doi.org/10.1038/s41561-018-0198-1.

Lavier, L.L., Manatschal, G., 2006. A mechanism to thin the continental lithosphere at magma-poor margins. Nature 440, 324–328.

Li, C.F., Lin, J., Kulhanek, D.K., the Expedition 349 Scientists, 2015. In: Proceedings of the International Ocean Discovery Program, vol. 349, South China Sea Tectonics. International Ocean Discovery Program, College Station, TX.

Li, C.F., Xu, X., Lin, J., Sun, Z., Zhu, J., Yao, Y.J., Zhao, X.X., Liu, Q.S., Kulhanek, D.K., Wang, J., Song, T.R., Zhao, J.F., Qiu, N., Guan, Y., Zhou, Z., Williams, T., Bao, R., Briais, A., Brown, E., Chen, Y., Clift, P., Colwell, F., Dadd, K., Ding, W., Almeida, I., Huang, X., Hyun, S., Jiang, T., Koppers, A., Li, Q., Liu, C., Liu, Z., Nagai, R., Peleo-Alampay, A., Su, X., Tejada, M., Trinh, H., Yeh, Y., Zhang, C., Zhang, F., Zhang, G., 2014. Ages and magnetic structures of the South China Sea constrained by deep tow magnetic surveys and IODP Expedition 349. Geochem. Geophys. Geosyst. 15 (12), 4958–4983. https://doi.org/10.1002/2014gc005567.

Liang, Y., Delescluse, M., Qiu, Y., Pubellier, M., Chamot-Rooke, N., Wang, J., Nie, X., Watremez, L., Chang, S., Pichot, T., Savva, D., Meresse, F., 2019. Decollements, detachments and rafts in the extended crust of Dangerous Ground, South China Sea: the role of inherited contacts. Tectonics. https://doi.org/10.1029/2018TC005418.

Lizaralde, D., Axen, G.J., Brown, H.E., Fletcher, J.M., Gonzalez-Fernandez, A., Harding, A.J., Holbrook, W.S., Kent, G.M., Paramo, P., Sutherland, F., Umhoefer, P.J., 2007. Variation in styles of rifting in the Gulf of California. Nature 448, 466–469.

Minshull, T.A., Dean, S.M., White, R.S., Whitmarsh, R.B., 2001. Anomalous melt production after continental breakup in the southern Iberia Abyssal plain. In: Wilson, R.C.L., Whitmarsh, R.B., Taylor, B., Froitzheim, N. (Eds.), Non-Volcanic Rifting of Continental Margins: A Comparison of Evidence from Land and Sea. In: Special Publication, vol. 187. Geological Society, London, pp. 537–550.

Nielsen, T.K., Hopper, J.R., 2004. From rift to drift: mantle melting during continental breakup. Geochem. Geophys. Geosyst. 5 (7), Q07003. https://doi.org/10.1029/2003GC000662.

Paton, D.A., Pindell, J., McDermott, K., Bellingham, P., Horn, B., 2017. Evolution of seaward-dipping reflectors at the onset of oceanic crust formation at volcanic passive margins: insights from the South Atlantic. Geology 45, 439–442.

Péron-Pinvidic, G., Manatschal, G., Minshull, T.A., Sawyer, D.S., 2007. Tectonosedimentary evolution of the deep Iberia-Newfoundland margins: evidence for a complex breakup history. Tectonics 26, TC2011.

Skogseid, J., 2001. Volcanic margins: geodynamics and exploration aspects. Mar. Pet. Geol. 18, 457–461. https://doi.org/10.1016/S0264-8172(00)00070-2.

Stica, J.M., Zalan, P.V., Ferrari, A.L., 2014. The evolution of rifting on the volcanic margin of the Pelotas Basin and the contextualization of the Parana-Etendeka LIP in the separation of Gondwana in the South Atlantic. Mar. Pet. Geol. 50, 1–21.

Sun, Z., Jian, Z., Stock, J.M., Larsen, H.C., Klaus, A., AvRarez Zarikian, C.A., the Expedition 367/368 Scientists, 2018. In: Proceedings of the International Ocean Discovery Program, vol. 367/368, South China Sea Rifted Margin. International Ocean Discovery Program, College Station, TX.

Sutra, E., Manatschal, G., Mohn, G., Unternehr, P., 2013. Quantification and restoration of extensional deformation along the Western Iberia and Newfoundland rifted margins. Geochem. Geophys. Geosyst. https://doi.org/10.1002/ggge.20135.

Taylor, B., Hayes, D.E., 1983. Origin and history of the South China Sea basin. In: Hayes, D.E. (Ed.), The Tectonic and Geologic Evolution of the Southeast Asian Seas and Islands: Part 2. In: Geophys. Monogr., vol. 27. AGU, Washington, DC, pp. 23–56.

Trude, J., Cartwright, J., Davies, R.J., Smallwood, J., 2003. New technique for dating igneous sills. Geology 31, 813–816.

Tugend, J., Gillard, M., Manatschal, G., Nirrengarten, M., Harkin, C., Epin, M.E., Sauter, D., Autin, J., Kusznir, N., McDermott, K., 2018. Reappraisal of the magma-rich versun magma-poor rifted margin archetypes. In: McClay, K.R., Hammerstein, J.A. (Eds.), Passive Margins: Tectonic, Sedimentation and Magmatism. In: Special Publications, vol. 476. Geological Society, London.

Wang, J.B., Pang, X., Liu, B., Zhen, J., Wang, H., 2018. The Baiyun and Liwan Sags: two supradetachment basins on the passive continental margin of the northern South China Sea. Mar. Pet. Geol. 95, 206–218.

Welford, J.K., Smith, J.A., Hall, J., Deemer, S., Srivastava, S.P., Sibuet, J.C., 2010. Structure and rifting evolution of the northern Newfoundland Basin from Erable multichannel seismic reflection profiles across the southeastern margin of Flemish Cap. Geophys. J. Int. 180, 976–998. https://doi.org/10.1111/j.1365-246X.2009.04477.x.

White, R.S., McKenzie, D., O'nions, R.K., 1992. Oceanic crustal thickness from seismic measurements and rare earth element inversions. J. Geophys. Res. 97, 19682–19715. https://doi.org/10.1029/92JB01749.

Whitmarsh, R.B., Manatschal, G., Minshull, T., 2001. Evolution of magma-poor continental margins from rifting to seafloor spreading. Nature 413, 150–154.

Yan, P., Zhou, D., Liu, Z., 2001. A crustal structure profile across the northern continental margin of the South China Sea. Tectonophysics 338 (1), 1–21.

Zhao, F., Alves, T.M., Wu, S., Li, W., Huuse, M., Mi, L., Sun, Q., Ma, B., 2016. Prolonged post-rift magmatism on highly extended crust of divergent continental margins (Baiyun Sag, South China Sea). Earth Planet. Sci. Lett. 445, 79–91.

Zhao, Y., Ren, J., Pang, X., Yang, L., Zheng, J., 2018. Structural style, formation of low angle normal fault and its controls on the evolution of Baiyun Rift, northern margin of the South China Sea. Mar. Pet. Geol. 89 (3), 687–700. https://doi.org/10.1016/j.marpetgeo.2017.11.001.

Zou, H.P., Li, P.L., Rao, C.T., 1995. Geochemistry of Cenozoic volcanic rocks in Zhujiangkou basin and its geodynamic significance. Geochimica 24 (S1), 33–45.